Materials Advances

ROYAL SOCIETY OF CHEMISTRY

PAPER

View Article Online
View Journal

Check for updates

Cite this: DOI: 10.1039/d6ma00392c

Boosted electron transfer kinetics in a rGO–Fe_3O_4/TiO_2 nanocomposite toward trace-level detection of chloramphenicol

Sidra Bibi,[a] Sadia Muzammal,[b] Safeer Ahmad,[a] Muhammad Siddiq,[a] Syed Sakhawat Shah,[a] Adnan Ashraf,[c] M. I. Khan[d] and A. Ahmad*[ce]

The quick and efficient analysis of antibiotic residues in food and environmental samples is a major challenge. In the current work, a ternary rGO–Fe_3O_4/TiO_2 nanocomposite was prepared and used as an effective electrocatalytic sensing platform to electrochemically detect chloramphenicol (CAP). The synergistic co-assembly of the conductive reduced graphene oxide (rGO), redox-active Fe_3O_4 NPs, and semiconducting TiO_2 was able to create a heterostructured interface to allow fast transfer of electrons and increase surface-active sites. The success of the hybrid nanocomposite with the uniform dispersion of metal oxides all over the rGO sheets was confirmed with the help of structural and morphological characterization. Electrochemical studies revealed a large reduction in current towards CAP as opposed to that of the single components, and this is a strong sign of electrocatalytic activity. The modified electrode was found to have high sensitivity, a large linear detection range, a low detection limit, excellent repeatability, and reasonable selectivity in the presence of possible interfering species. In particular, quantitative parameters like the limit of detection (LOD = 0.88 μM), limit of quantification (LOQ = 2.95 μM), sensitivity (4.01 μA μM^{-1} cm^{-2}), linear range of detection (2–100 μM), relative standard deviation (RSD = 1.79%) in reproducibility. These extensions give a more accurate picture of the sensor in terms of its analytical capabilities and usability. The findings provide a more concise emphasis on the importance, robustness, and sensitivity of the developed rGO–Fe_3O_4/TiO_2-based electrochemical sensor to detect chloramphenicol. Moreover, the sensor was found to be stable in real sample analysis, which implies its potential use in environmental and food safety monitoring. The synergistic interactions between charge-transfer and the higher adsorption capacity of the rGO–Fe_3O_4/TiO_2 ternary system are responsible for the enhanced sensing performance.

Received 19th March 2026,
Accepted 16th April 2026

DOI: 10.1039/d6ma00392c

rsc.li/materials-advances

Open Access Article. Published on 05 June 2026. Downloaded on 6/15/2026 10:28:08 PM.
This article is licensed under a Creative Commons Attribution 3.0 Unported Licence.

1. Introduction

A well-known antibiotic with action against both Gram-negative and Gram-positive bacteria is chloramphenicol (CAP). Before the year 2020, CAP was frequently used to treat bacterial infections in animals, such as TB.[1] Unfortunately, CAP has evolved into a common contaminant in a variety of environments, including soil, water, and food.[2] CAP particularly poses a risk to human health since it can accumulate in the body and cause a few illnesses, including leukaemia, aplastic anaemia, grey baby syndrome, and bone marrow suppression. The maximum permitted absorption of CAP in beef commodities for human health is 0.3 μg kg^{-1}. CAP is a normal organic molecule in chemical perception, which can be examined using high-performance liquid chromatography (HPLC), liquid chromatography-mass spectrometry (LCMS), spectrofluorimetry, and electrochemical analysis. Nevertheless, such techniques are disadvantageous, including being time-consuming, expensive, and necessitating pretreatment of the samples. They have low sensitivity and selectivity that restrict their use in certain cases. Anodic stripping voltammetric methods (ASV) have been identified as efficient methods of analyzing inorganic and organic compounds due to many advantages that they offer, such as improved speed, increased selectivity and sensitivity, reduced cost, reduced detection limit, and the ability to conduct analysis on site. Differential pulse-anodic stripping voltammetry

[a] Department of Chemistry, Quaid-i-Azam University, Islamabad, Pakistan
[b] Key Laboratory of Green Chemical Media and Reactions, Ministry of Education Collaborative Innovation Center of Henan Province for Green Manufacturing of Fine Chemical, School of Chemistry and Chemical Engineering, Henan Normal University, Xinxiang, 453007, Henan, China
[c] Department of Chemistry, The University of Lahore, Lahore, Pakistan. E-mail: awaisahmed@gcuf.edu.pk
[d] Department of Physics, The University of Lahore, Lahore, Pakistan
[e] Faculty of Engineering and Technology, Shinawatra University, Sam Khok, Thailand

© 2026 The Author(s). Published by the Royal Society of Chemistry

Open Access Article. Published on 05 June 2026. Downloaded on 6/15/2026 10:28:08 PM. This article is licensed under a Creative Commons Attribution 3.0 Unported Licence.

(DPASV), which is one type of ASV technique, has been applied to estimate various organic compounds due to their complex structures and low chemical reactivity. Therefore, the development of highly effective detection methods for CAP detection is necessary.[3]

To date, a few analytical techniques, including liquid chromatography,[4] colorimetry,[5] and electrochemistry,[6,7] have been established for CAP detection. Due to its benefits of quick reaction, cheap cost, simplicity, and high sensitivity, electrochemical technology has been identified as one of the technologies that exhibit promising results in real-world applications.[8] The sensing performance of electrochemical CAP sensors is strongly affected by the physiochemical properties of the sensing materials (electrocatalysts), in general. Consequently, the fabrication of new electrocatalysts that possess high catalytic selectivity and high conductivity is critical towards creation of efficient CAP sensors.[9]

A nanomaterial's formulation can be categorized into three forms: physical, chemical and green method,[10] from which inorganic, organic and carbon-based nanomaterials are synthesized. Since carbon nanomaterials can be advantageous in terms of their high conductivity and ability to be customized in structure, they have recently been determined as potentially useful in the development of high-performance electrochemical sensors.[11] Actually, different types of carbon nanomaterials have been utilized as a platform to prepare entirely novel sensing substances towards CAP detection electrochemically. $SmMoSe_2$@GO has been utilized as a graphene oxide (GO) support of CAP sensors due to its two-dimensional (2D) layered structure,[12] along with $Ce(MoO_4)_2$/GO, AuNPs/GO, AuNPs/N–rGO, rGO–Pt–Pd NCs, Sr–ZnO@rGO, PdNPs/rGO, and Co_3O_4rGO.[13,14] Multi-walled carbon nanotubes (MWCNTs) are also used as a common one-dimensional (1D) conductive carbon nanomaterial towards electrochemical sensing of CAP, with reported sensing materials such as MoS_2-coated MWCNTs, and MWCNT–CTAB–PDPA.[15] Carbon black (CB), a standard high-quality carbon support of electrochemically active sites to detect CAP, has also been used to support electrochemically active sites. MIL-101(Cr)/XC-72 and MoS_2/CB[16] both have good sensing performances in CAP electrochemical detection. Other carbon-based electrochemical CAP detections have also been reported recently, including those using MoN nanorods/sulfur-doped graphitic carbon nitrate, flower-like $MnWO_4$ on defect-engineered graphitic carbon nitrate (g-C_3N_4), ordered mesoporous carbon@polydopamine, semi-graphitic sulfur-doped ordered mesoporous carbon material, and MOF-derived exfoliated porous carbon.[17–19]

It is believed that carbon-based functional materials may serve as a potential metal-free material in terms of energy and environmental use, as per existing literature. As an example, Bonomo and co-authors proved that bioactive compounds may be applied in processes that involve the use of dye-sensitized solar cells (DSSCs) as cost-effective and eco-friendly components.[1,20] Bella *et al.* designed two types of poly(ethylene glycol)-based units, which are divided by the use of a perfluorinated barrier in order to store energy in DSSCs and store charges in EDLCs.[21] PEMFCs and CF-SOFCs both use materials based on carbon as fuels in the gas diffusion layer of fuel cells.[22,23] The cationic poly(3,4-ethylenedioxythiophene) (PEDOT) derivative, cathode of aqueous solar cells, records an efficiency of 7.02%.[24,25] In the use of wearable supercapacitors, MoS_2 and Cu_7S_4-decorated graphene aerogels have been used as active materials. Considering this, carbon-containing materials possess some special properties that enable them to be excellent energy and environmental materials, thus providing valuable insight into the rational engineering of high-performance sensing materials to develop CAP sensors.[26]

Chloramphenicol (CAP) is an example of a broad-spectrum antibiotic commonly used in veterinary and aquaculture applications, but its toxicological characteristics, such as bone marrow suppression and aplastic anemia, are so severe that it has very strict regulatory restrictions and zero-tolerance limits in food and environmental matrices. CAP is highly polarized and persists very well and is therefore very difficult to detect at a trace level. The traditional methods of analysis (HPLC, GC, and LC-MS) are effective, but have certain shortcomings, such as an expensive nature, a lengthy process, and intricate sample preparation.[27] Conversely, electrochemical sensing has become a viable alternative because of its quick reaction, high sensitivity, portability, and low cost of operation, which are highly appropriate in on-site monitoring of antibiotic residues. The redox conversion of the nitro group of CAP is the key to electrochemical detection of the amino acid, and quantification of chemical compound can be performed sensitively through the distinct reduction peaks.[28]

The working of electrochemical sensors is highly determined by the physicochemical characteristics of electrode materials, and nanostructured materials are very important in improving sensitivity and selectivity. Specifically, carbon-based substances, including reduced graphene oxide (rGO), have an outstanding electrical conductivity, a high surface area, and π–π interaction capacity, allowing them to transfer electrons rapidly and adsorb aromatic analytes, such as CAP.[29] In the meantime, metal and metal oxide nanoparticles (*e.g.*, Fe_3O_4, TiO_2, ZnO, and Pd) add a lot of catalytically active sites, better electrocatalytic activity, and more charge-transfer kinetics.[30] Combining these elements into hybrid nanocomposites forms synergetic heterostructures that can greatly enhance the sensing performance by enhancing the electroactive surface area, accelerating electron mobility, and enhancing the interaction of the analyte.

Recent investigations have revealed that different nanocomposites are effective in CAP detection. To illustrate, GO/ZnO hierarchical nanocomposites were highly sensitive (7.27 μA μM^{-1} cm^{-1}) and have low detection limits (0.01 μM) because of their increased surface area and conductivity. In same way, rGO coated with Pd nanoparticles attained detection limits down to 50 nM, which is due to the enhanced electrocatalytic activity and electron transfer efficiency.[31] More complicated hybrid materials like lignocellulosic carbon/GO@MnO_2 and MOF/rGO have also demonstrated even lower detection limits in nanomolar range,[32] underscoring the power

© 2026 The Author(s). Published by the Royal Society of Chemistry

Open Access Article. Published on 05 June 2026. Downloaded on 6/15/2026 10:28:08 PM. This article is licensed under a Creative Commons Attribution 3.0 Unported Licence.

of synergistic design of materials. These investigations strongly suggest that the incorporation of conductive carbon structures with catalytically active metal or metal oxide nanostructures is an effective approach towards high-performance electrochemical sensors.

There is no question that the addition of carbon nanomaterials to the sensing components for electrochemical CAP sensors results in improved sensing performance, especially when compared to sensing system without carbon nanomaterials.[33] Notably, there were noticeable differences in physical and chemical characteristics of the carbon nanomaterials mentioned above. Previous studies have demonstrated that three common carbon nanomaterials, namely rGO, MWCNTs, and CB, have distinctly diverse sensing capacities for the detection of glucose and electrochemical activity for reduction of oxygen.[34] As per our concern, there haven't been many reports of comparative studies of the impact of different carbon nanomaterials on electrochemical CAP detection. Inspired by these innovations, the current study aims at designing a ternary rGO–Fe_3O_4/TiO_2 nanocomposite, in which the conduction network of rGO, redox of Fe_3O_4, semiconducting, and adsorption of TiO_2 are integrated synergistically to improve the electron transfer kinetics and detection of CAP.

Herein, the present work focuses on insight into effect of the carbon support on electrochemical CAP sensors. Carbon nanomaterials, like rGO, were used as a carbon support for further deposition of trace Fe_3O_4/TiO_2, leading to preparation of sensing materials for CAP sensors. Fe_3O_4 and TiO_2 nanoparticles were selected to modify the carbon supports because recent research showed that Fe_3O_4 and TiO_2 nanoparticles exhibit good catalytic activity for the electrochemical detection of CAP. By combining structural characterization of carbon-based sensing materials and sensing performance analysis of the corresponding CAP sensors, it was found that sensing performances are strongly dependent on microstructures of carbon supports. The rGO–Fe_3O_4/TiO_2-based electrochemical sensor has been developed to detect the pharmaceutical antibiotic drug CAP in a standard solution, as well as in a common eye drop chloroptic as a practical sample. For the detection of CAP, a detailed explanation is given in the subsequent sections.

2. Materials and methods

2.1 Materials

Analytical grade ethanol (C_2H_5OH: 97%), sodium nitrate ($NaNO_3$: 99%), sulfuric acid (H_2SO_4: 95–97%), graphite powder (99%), potassium permanganate ($KMnO_4$: 99%), hydrochloric acid (HCl: 37%), hydrogen peroxide (H_2O_2: 30%), titanium tetra isopropoxide (TTIP: 97%), acetic acid (CH_3COOH: 99%), ferric chloride ($FeCl_3{\cdot}6H_2O$: 97%), ferrous chloride ($FeCl_2{\cdot}4H_2O$: 97%), and chloramphenicol ($C_{11}H_{12}C_{l2}N_2O_5$: 98%) were all bought from Sigma Aldrich and used without supplementary refinement. All the solutions were prepared using deionized water (DI).

2.2 Synthesis of rGO, TiO_2, and rGO–Fe_3O_4/TiO_2

To prepare graphene oxide, modified Hummers' method was utilized, in which 2 g of graphite flakes and 2 g of $NaNO_3$ were combined in 50 mL of H_2SO_4 in a 1000 mL round-bottom flask, and suspension was mixed vigorously for 60 min in an ice bath (5 °C).[35] Moreover, 6 g of $KMnO_4$ was dropwise added to suspension, and mixture was stirred continuously until reaction color changed to green and temperature was constant at 15 °C. The mixture was stirred at 35 °C for 24 h to change the color of the mixture to pastry brown, then 100 mL of H_2O was added gradually to suspension, and reaction temperature was raised to 98 °C, and a brown color was observed. This was followed by the addition of 200 mL of cold water under stirring and finally by the addition of H_2O_2 (10 mL). Finally, to purify it, 10% HCl was added, after which it was washed with DI water until the pH of solution was neutral and subsequently dried in oven at 60 °C.

In addition, rGO was prepared by exfoliating 0.1 g of GO in 100 mL of water using an ultrasonic water bath over 12 h at a temperature of 50 °C.[36] 0.15 g of ascorbic acid was put into the suspension of GO and stirred over a period of 12 h at 50 °C. In the last step, the precipitates of rGO were acquired. This rGO was rinsed with ethanol, followed by centrifugation and 80 °C vacuum oven drying over 5 h. Modified sol gel method was used to synthesized pure TiO_2. Two solutions were made, solution one was made by mixing 0.1 M titanium isopropoxide with 100 mL of ethanol and solution two was by mixing the ethanol, acetic acid and water in ratio of 7 : 3 : 1. Then solutions 1 and 2 were mixed by adding solution 1 slowly into 2 under continuous stirring till 6–8 hours. Afterwards solution mixer was aged at room temperature for overnight. Then gel was dried in oven and successively calcined for 3 hours at 500 °C. Two steps modified method was used to synthesized ternary rGO–Fe_3O_4 /TiO_2 nanocomposite. At first in 100 mL of DI water 50 mg of rGO was dispersed and for 1 hour successively stir the solution. Afterwards Fe_3O_4 solution (10 mL) was poured in rGO solution and continued on stirring for 3 hours. Successively sample was washed and dried for 12 hours at 110 °C. After that in 25 mL of DI water 50 mg of rGO–Fe_3O_4 was dispersed under sonication for 1 h and then added specific amount of TiO_2 in rGO–Fe_3O_4 solution. Successively, above mixture was added in autoclave and heated for 6 hours at 180 °C. After cooling, washed sample using DI water throughly and sample was allowed to dried for 12 hours at 110 °C. This process we already descirbed in our previous study.[37]

2.3 Characterization

For the electrochemical measurements, cyclic voltammetry was carried out using the Gamry Interface 1000E Potentiostat electrochemical workstation. Using a three-electrode cell arrangement with a glassy carbon electrode (GCE) as a working electrode (working area = 0.071 cm^2), Ag/AgCl as a reference electrode, and Pt wire as a counter electrode, all electrochemical measurements were performed.

2.4 Fabrication of the modified electrode

Before rGO, TiO_2, and rGO–Fe_3O_4/TiO_2 composite modification on the GCE, the GCE was well polished with 0.05 μM alumina

Open Access Article. Published on 05 June 2026. Downloaded on 6/15/2026 10:28:08 PM. This article is licensed under a Creative Commons Attribution 3.0 Unported Licence.

slurry. Then, 5 mg mL^{-1} of the as-prepared composite was redispersed in DI water. Afterward, about 8 μL (optimized concentration) of rGO, TiO_2, and the rGO–Fe_3O_4/TiO_2 composites were drop-cast on the mirror-polished GCE; after that, it was allowed to dry at room temperature.[38] The obtained rGO–Fe_3O_4/TiO_2/GO/GCE was used for further electrochemical measurements.

Table 1 The parameters calculated from the cyclic voltammogram and Nyquist plot

Nominal	ESA (cm^2)	R_{CT} (kΩ)	R_s (kΩ)	W_d (μF)
GCE	0.01	3.9	0.04	30
TiO_2/GCE	0.02	3.5	0.13	151
rGO–Fe_3O_4/GCE	0.03	0.66	0.09	159
rGO–Fe_3O_4–TiO_2/GCE	0.05	0.8	0.11	145

3. Results and discussion

3.1 Characterization of rGO, TiO_2, and rGO–Fe_3O_4/TiO_2

Physical characterization studies like XRD, FTIR, SEM, EDX, and TGA were done and discussed in our previous article.[37]

3.1.1 CV and EIS characterization of the bare and modified GCE. The electrochemically active surface area of the GCE, TiO_2/GCE, and rGO–Fe_3O_4/TiO_2/GCE modified electrode was estimated by applying cyclic voltammetry (CV) in the model redox system of 5 mM K_3[Fe $(CN)_6$] in 0.1 M KOH solution. As shown in Fig. 1(a), rGO–Fe_3O_4/TiO_2/GCE produced the highest peak current. Based on these results, ESA was estimated using the Randles–Sevcik equation (eqn (1)), and the results are listed in Table 1, indicating the highest ESA for rGO–Fe_3O_4/TiO_2/GCE.

$$I_p = 2.69 \times 10^5 \times n^{3/2} A C D^{1/2} \nu^{1/2} \quad (1)$$

EIS measurements were performed using GCE, TiO_2/GCE, and rGO–Fe_3O_4/TiO_2/GCE in a model redox system of 5 mM K_3[Fe $(CN)_6$] in 0.1 M KOH solution within a frequency range of 0.1 Hz to 100K Hz.[39,40] The Nyquist plots of the EIS spectra of the GCE, TiO_2/GCE, and rGO–Fe_3O_4/TiO_2/GCE are displayed in Fig. 1(b). All obtained data were fitted in the equivalent circuit CPE with diffusion, and results are listed in Table 1. A small semicircle domain was observed for rGO–Fe_3O_4/TiO_2/GCE, indicating a lower charge-transfer resistance (R_{ct}) than for TiO_2/GCE, as shown in Table 1. Both the large ESA and low charge-transfer resistance (R_{ct}) suggest that rGO–Fe_3O_4/TiO_2/GCE serves as a promising platform for electrochemical detection.[41] The TiO_2 in composite will play an expected role in the overall electrocatalytic behaviour of the composite, as it gives it extra active sites and enables the surface adsorption of molecules in analyte. Besides, it can be integrated with conductive rGO and Fe_3O_4 to improve interfacial charge transfer. Nevertheless, a focus on contribution of TiO_2 in this study was not isolated, and rather it was deduced by the electrochemical characteristics observed and literature findings.

This is because the charge-transfer resistance of rGO–Fe_3O_4/TiO_2/GCE can be significantly reduced by the excellent electron conduction of rGO and its π-conjugated structure, which provides good electron conduction channels. The strong interfacial interaction between rGO and Fe_3O_4/TiO_2 NPs facilitates rapid charge transfer and reduces interfacial resistance.[42] In addition, due to the high surface area of rGO, dispersion of metal oxide nanoparticles is more uniform and, as a result, the electroactive sites on the electrode–electrolyte interface increase, as well as overall electron transfer dynamics.[43] The improved sensing performance has been explained by the fact that the rGO–Fe_3O_4/TiO_2 composite has better electron transfer kinetics and an extended active surface area. This meaning is confirmed by electrochemical studies (EIS and CV), but specific mechanistic hints like the adsorption behavior and identification of intermediates were not in the scope of the present investigation.

3.2 Electrochemical behavior of chloramphenicol

The electrochemical response of CAP was investigated on GCE, modified TiO_2/GCE, and rGO–Fe_3O_4 TiO_2/GCE in 0.5 M phosphate buffer (PB) as electrolyte and in PB containing 0.2 mM CAP at a scan rate of 100 mV s^{-1} displayed in Fig. 2(a and b). At the GCE, modified TiO_2/GCE, and rGO–Fe_3O_4 TiO_2 modified

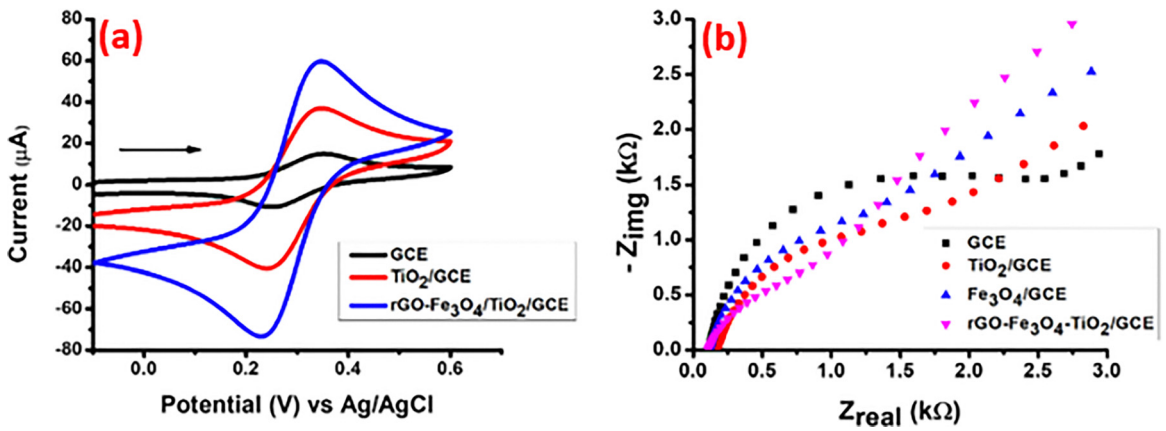

Fig. 1 (a) Cyclic voltammogram of TiO_2/GCE and rGO–Fe_3O_4 TiO_2/GCE; (b) Nyquist plot recorded at the (black) GCE, (red) TiO_2/GCE, and (blue) rGO–Fe_3O_4 TiO_2/GCE.

© 2026 The Author(s). Published by the Royal Society of Chemistry

Open Access Article. Published on 05 June 2026. Downloaded on 6/15/2026 10:28:08 PM.
This article is licensed under a Creative Commons Attribution 3.0 Unported Licence.

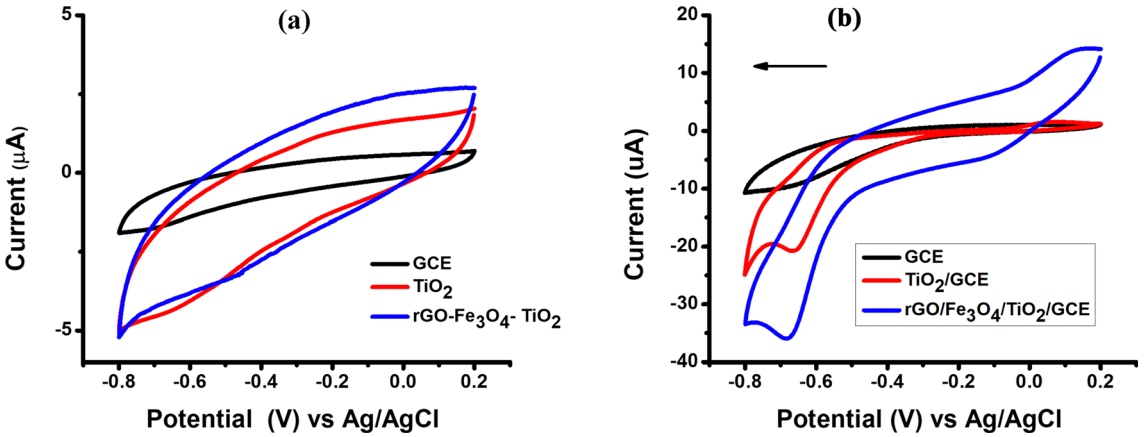

Fig. 2 CV of TiO_2/GCE and rGO–Fe_3O_4/TiO_2/GCE in the (a) absence of CAP in PB (pH = 7) and (b) presence of 0.2 mM CAP/PB at a scan rate of 100 mV.

GCE in 0.5 M PB, no oxidation/reduction peak was observed. CV was also recorded from positive to negative potential in 0.5 M PB containing 0.2 mM CAP, with TiO_2/GCE and rGO–Fe_3O_4/TiO_2/GCE. CAP showed irreversible behavior with two reduction peaks at $E_{pA} = -0.67$ V and $E_{pB} = -0.051$ V, and one oxidation peak at 0.1 V.[44,45] However, the higher reduction peak current on rGO–Fe_3O_4/TiO_2/GCE at peak A corresponds to four-electron irreversible reduction of nitro group of CAP to a hydroxylamine group. Furthermore, a two-electron reversible redox reaction of hydroxyl group was found at peaks B_1 and B_2 to give a nitroso derivative of CAP. Maximum peak current was found in the cathodic region, so the irreversible reduction peak A has been chosen for the estimation of CAP.[46,47]

The morphological characteristics of synthesized metal oxide/rGO composite were previously studied in detail in our previous work.[37] SEM images were acquired at high resolution; the metal oxide nanoparticles were uniformly dispersed on the rGO sheets, and a clear heterostructured interface was observed, with no agglomeration. As the present work is devoted to assessing the biosensing properties of a material that has already been synthesized, detailed structural characterization is not presented here; interested readers can consult our previous report for a detailed microscopic examination of the material.

3.3 Optimization of the experimental conditions

To achieve the maximum current response, the experimental conditions were optimized. Details are given below.

3.3.1 pH effect. Generally, in volumetric analysis, selection of buffer solution is important. The electrolyte pH significantly affects the electrochemical behavior of analyte because protons are subsequently involved in electron transfer process and have a serious effect on peak potential and peak current. Reduction of CAP peak current was examined by applying CV in pH range of 4–10 of standard electrolyte containing 0.2 mM CAP at a scan rate of 100 mV s^{-1} as shown in Fig. 3(a). With the subsequent increase in pH of electrolyte (PB), cathodic peak potential shifted toward a more negative value when pH increases from 4 to 10. The maximum peak current was observed at pH 7, while the peak current was decreased above or below pH 7, as illustrated in Fig. 3(b), so pH 7 was chosen for further electrochemical analysis.[48] Cathodic peak potential was plotted *versus* pH (Fig. 3(c)) with the linear regression eqn (2). The value of slope, 43 mV pH^{-1}, indicates that an equal number of electrons and protons are transferred to electrode surface.[49,50] As pH increased, peak potential moved to give a negative slope of 43 mV pH^{-1}. This value is marginally lower than the theoretical Nernstian slope of 59 mV pH^{-1}, which would have occurred with an equivalent number of protons and electrons, but deviations are common in nanomaterial-modified electrodes because of the quasi-reversible electron transfer kinetics and surface adsorption effects. This trend indicates that the electrochemical reaction follows a proton-coupled electron transfer reaction. E_p-pH behavior followed the following linear regression equations:

$$E_{pc}\ (V) = -0.344 - 0.041pH \quad (R^2 = 0.99) \qquad (2)$$

Eqn (2) is for the reduction peak current of CAP, with the value of $R^2 = 0.99$, which shows the linear relationship between the peak potential and pH of the solutions.

The concentration of electrochemical sensor is critical for detecting drugs on electrode surface. The optimum concentration of sensor generally increases ESA, enhances electron transfer and decreases the charge transfer resistance. Herein we used different concentrations of sensor (RFT), namely 0.2 mg mL^{-1}, 0.3 mg mL^{-1}, 0.4 mg mL^{-1}, 0.5 mg mL^{-1}, and 0.6 mg mL^{-1}, to get the optimum concentration of our sensor as presented in Fig. 3(d) and (e). Maximum reduction peak current was obtained by 0.5 mg mL^{-1} concentration. After that, the reduction peak current decreased, as higher concentration of sensor on the GCE may lead to poor adhesion or resistance. Furthermore, the optimum concentration of sensor is critical for maintaining the stability in real sample analysis.

3.3.2 Effect of scan rate/kinetic investigation. Information about nature of electrochemical reaction occurring on electrode surface, whether it is adsorption or diffusion controlled, kinetic parameters, and oxidation or reduction mechanism can be attained by plotting peak potential/current with scan rate relationship. Hence, the scan rate impact on the rGO/Fe_3O_4/TiO_2

Open Access Article. Published on 05 June 2026. Downloaded on 6/15/2026 10:28:08 PM.
This article is licensed under a Creative Commons Attribution 3.0 Unported Licence.

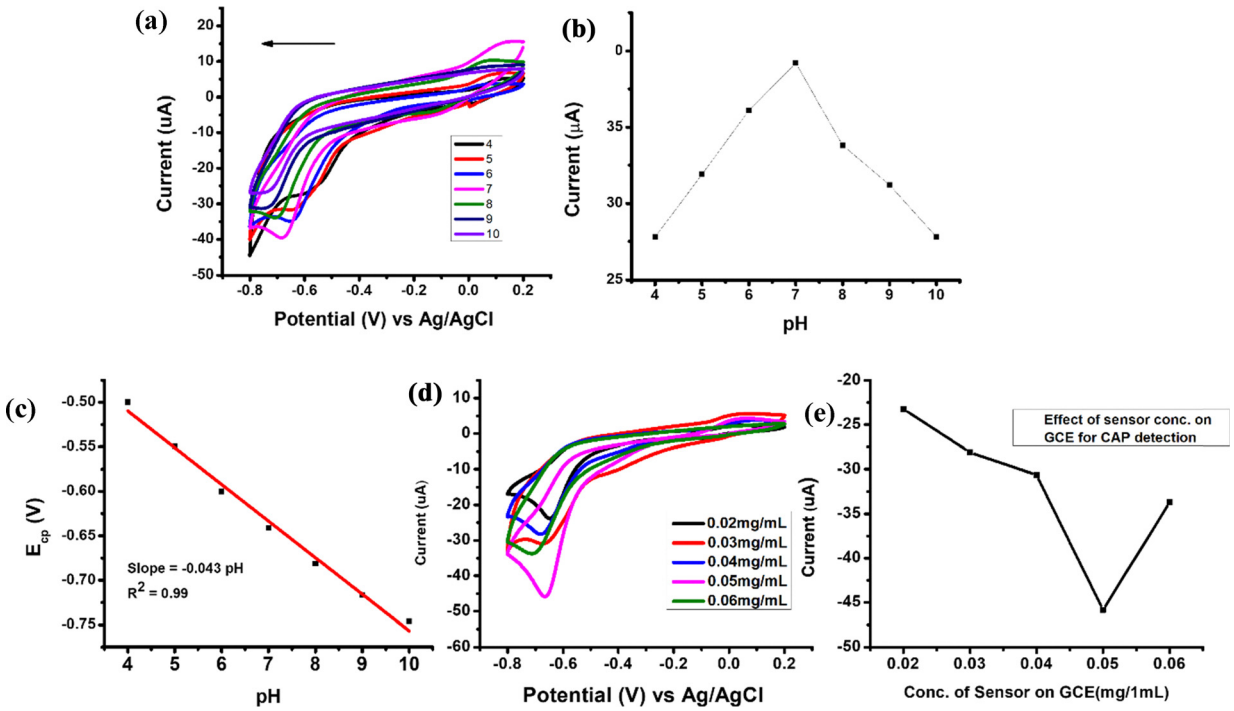

Fig. 3 (a) The CV response of the reduction peak at rGO–Fe_3O_4/TiO_2/GCE in a pH range of 4–10, (b) plot of peak current *vs.* pH, (c) plot of reduction peak potential (E_{pc}) *vs.* pH, and (d) and (e) optimum concentration of our sensor.

modified GCE toward reduction peak current of CAP was studied using CV in 0.05 M PB containing 0.2 mM CAP by changing the scan rate (10–150 mV s^{-1}) as shown in Fig. 4(a). It can be observed from the scan rate effect on CAP that an increase in scan rate intensity of peak current (I_{pc}) and shift of peak potential (E_{pc}) toward a positive value indicates irreversible nature of the electron transfer process.[51] The nature of electrode process can be confirmed by plotting the $\log I_{cp}$ *versus* $\log v$ and obtaining straight line according to given expression below (Fig. 4(c)).

$$\log I_{pc}\ (\mu A) = 0.32 \log v\ (\text{mV s}^{-1}) - 4.14 \quad (R^2 = 0.996) \qquad (3)$$

A slope value of $\log I_{pc}$ *versus* $\log v$ plot near 0.5 is attributed to a diffusion-controlled process, and one near 1 corresponds to an adsorption-controlled process. In eqn (3), value of slope is close to reported value of 0.5, which indicates that the process is diffusion-controlled.[52] Furthermore, the plot of peak current *versus* square root of scan rate is shown in Fig. 4(b), and its linear regression eqn (4) is expressed below.

$$I_{pc}\ (\mu A) = -2.52v^{1/2}\ (\text{mV s}^{-1})^{1/2} - 9.89 \quad (R^2 = 0.991) \qquad (4)$$

The diffusion characteristics of CAP reduction were further verified by linear dependence of intensity of peak current on the square root of scan rate, which can be depicted through a plot of I_{pc} *versus* $v^{1/2}$. Furthermore, the dependence of cathodic peak potential E_{cp} *versus* $\log v$ is depicted in Fig. 4(d) with linear regression eqn (5) and (6) for an irreversible system.[53]

$$E_{pc}\ (\text{V}) = -0.0275 \log v\ (\text{V s}^{-1}) - 0.7067 \quad (R^2 = 0.999) \qquad (5)$$

$$E_{pc}\ (\text{V}) = 0.0686 \log v\ (\text{V s}^{-1}) - 0.1081 \quad (R^2 = 0.999) \qquad (6)$$

The number of electrons can be calculated from the slopes of eqn (5) and (6), which are 4.29 and 1.78, respectively, indicating that 4 electrons are involved in irreversible reduction of nitro group of CAP, while 2 electrons are involved in reversible oxidation of hydroxylamine group of CAP. The results found that there were 4.29 and 1.78 electron transfer numbers of irreversible and reversible processes, respectively. Given the experimental uncertainty inherent in the experiment and approximate nature of these electrochemical models, these values were reasonably estimated to be four and two electrons, respectively, to get a mechanistic interpretation.

3.4 Analytical performance

3.4.1 Voltammetric determination. The dependence of cathodic peak current I_{pc} on concentration of CAP was investigated by employing differential pulse voltammetry (DPV) to determine practicability of developed sensor (rGO–Fe_3O_4/TiO_2). A dynamic relationship was observed under optimal conditions, as a function of CAP concentration and peak current (I_{pc}), as shown in Fig. 5(a). The regression equation (eqn (7)) was obtained by plotting I_p *versus* CAP concentration.

$$I_p = 0.1925X - 1.806(0.98) \qquad (7)$$

A sensitivity calculation has been included in the proper section of analytical performance. In particular, sensitivity has now been clearly defined and calculated based on the slope of calibration curve divided by electroactive surface area (sensitivity = slope/ESA) with a result of 4.01 μA μM^{-1} cm^{-1}. To enable clarity and reproducibility, this calculation has been explicitly given in the section of Analytical performance (voltammetric

© 2026 The Author(s). Published by the Royal Society of Chemistry

Open Access Article. Published on 05 June 2026. Downloaded on 6/15/2026 10:28:08 PM.
This article is licensed under a Creative Commons Attribution 3.0 Unported Licence.

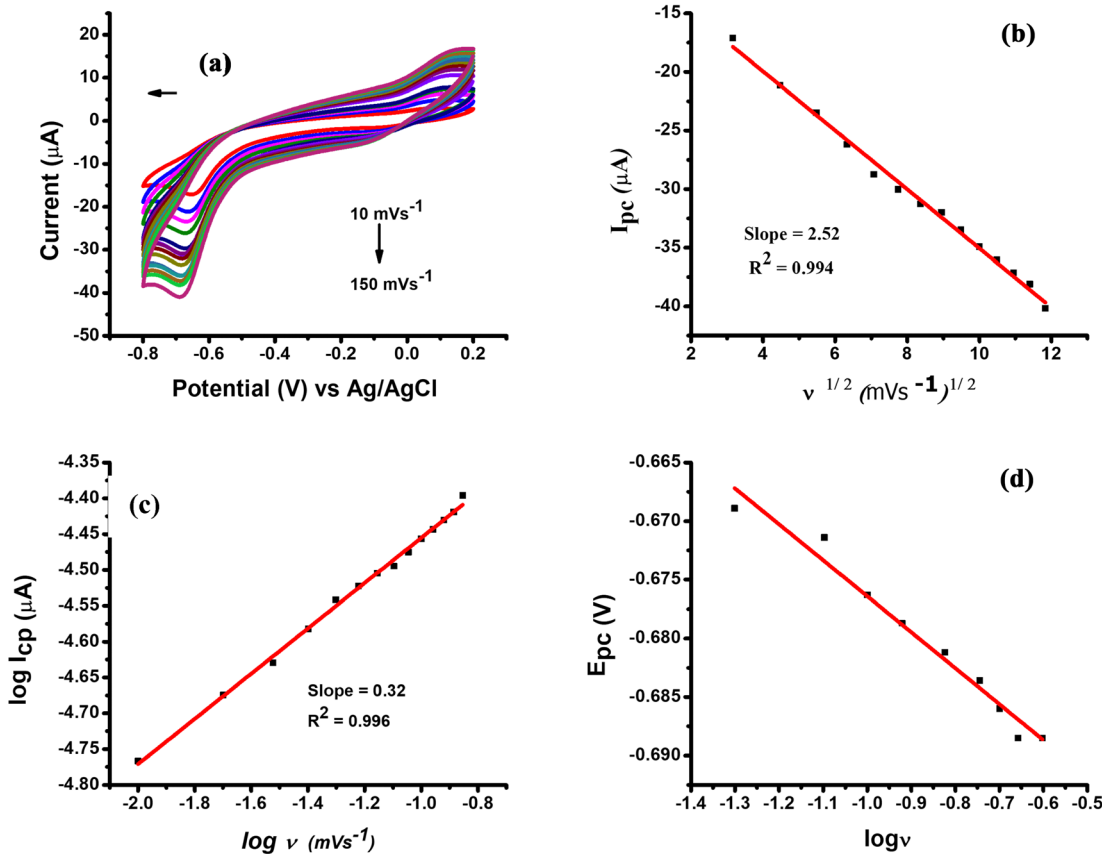

Fig. 4 (a) CV of the 0.2 mM CAP at rGO–Fe_3O_4/TiO_2/GCE with different scan rates (10–150 mV s^{-1}) in 0.05M PB of pH = 7, (b) plot of peak current *vs.* scan rate, (c) plot of log I_{cp} *vs.* log *v*, and (d) plot of E_{pa} *vs.* log *v*.

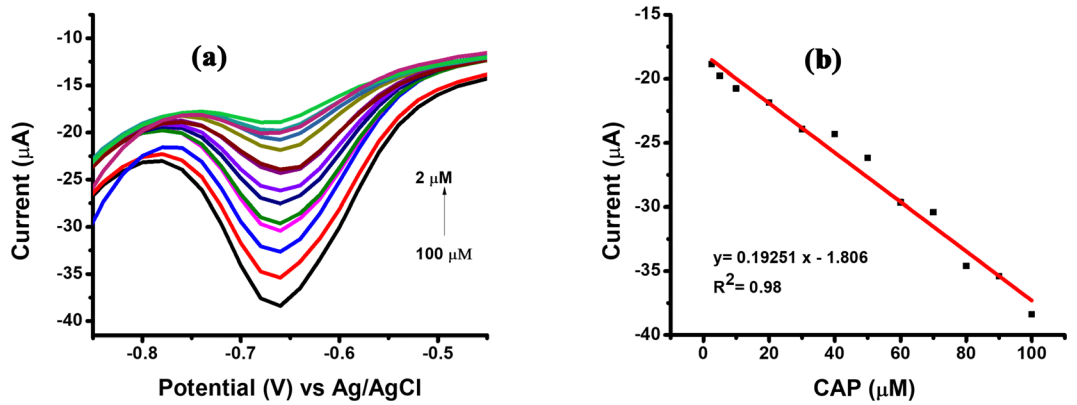

Fig. 5 (a) Differential pulse voltammogram of rGO–Fe_3O_4/TiO_2/GCE in PB (pH = 7) containing different concentrations of CAP, and (b) calibration plot of cathodic peak current *vs.* CAP concentration with rGO–Fe_3O_4/TiO_2/GCE.

determination) in addition to the calibration plot. Also, the corresponding value has already been given in Table 2 and briefly mentioned in abstract to bring out the analytical ability of sensor. This update will make sure that sensitivity is added, computed, and discussed appropriately with other important performance parameters. LOD and LOQ have been calculated from slope of calibration curve, as shown in Fig. 5(b), using equation 3 σ/slope and 10 σ/slope of the calibration curve, where σ is standard deviation of blank reading (8–10).[54] LOD and LOQ were found to be 0.88 μM and 2.95 μM, respectively, in concentration range of 2–100 μM. CAP was also determined in chloroptic eye drops with the RSD value of 0.12. The analytical curve parameters were calculated and listed in Table 2.

3.4.2 Interference study. The key parameter of interest in determining usefulness of an electrochemical sensor in practice is selectivity, especially when it comes to the complex

Table 2 Parameters calculated from the calibration curve

Formula	Calculated value	Sample	CAP (μM) Spiked	Found (μM)	Recovery (%)
LOD = $3\sigma/k$	0.88 μM	Eye drop	15	14.9	99
LOQ = $10\sigma/k$	2.95 μM	CAP	20	19.4	97
			26	25.7	98
			35	34.2	97
Sensitivity = slope/ESA	4.01 μA μM^{-1} cm^{-2}		39	38.5	98

Open Access Article. Published on 05 June 2026. Downloaded on 6/15/2026 10:28:08 PM. This article is licensed under a Creative Commons Attribution 3.0 Unported Licence.

environmental and food matrices where structurally related compounds and electroactive species can be present simultaneously. Anti-interference properties of the modified electrode made of rGO/Fe_3O_4/TiO_2 were explored systematically in presence of possible interfering substances, including ions (Na^+, K^+, Ca^{2+}, and Mg^{2+}), bio-related molecules (glucose, uric acid, ascorbic acid), and structurally related antibiotics.[55] The electrochemical reaction of CAP was observed following introduction of interfering species at a CAP concentration that is much higher.[56] The sensor showed low selectivity for CAP, as peak potential and peak current had very low variation. Some electroactive species, like organic compounds, and metal and non-metal ions, may interfere with performance of developed sensor. For evaluation of selectivity, it was observed that with 50 μM concentration of CAP, 25, 50, and 100 μM concentrations of ascorbic acid, glucose, Mg^{2+}, and K^+ don't interfere with determination of CAP, as depicted in Fig. 6. The low level of interference may be ascribed to a combination of several reasons:

✓ The π-conjugated rGO surface interacts more strongly with the nitroaromatic structure of CAP by π–π stacking.

✓ Synergistic catalytic sites: the catalytic specificity of Fe_3O_4 NPs is enhanced because of catalytic selectivity of nitro group of CAP.

✓ The rGO/Fe_3O_4/TiO_2 interface facilitates selective electron transfer kinetics of CAP reduction compared to other electroactive species.

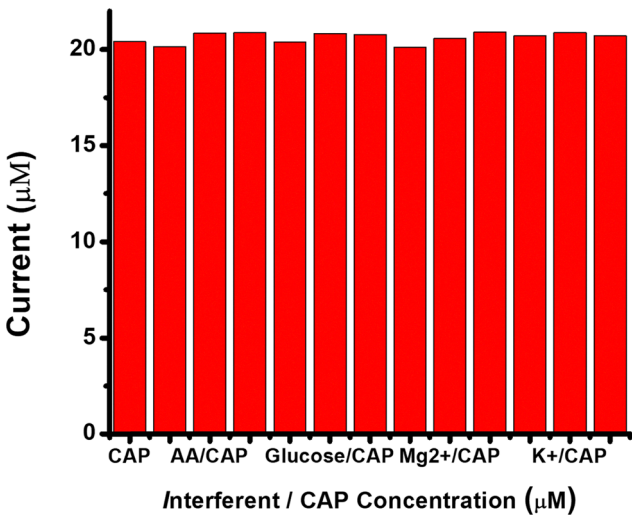

Fig. 6 Interference effect of 50 μM CAP with 25, 50, and 100 μM concentration of glucose, ascorbic acid, Mg^{2+}, and K^+.

✓ These findings affirm that ternary nanocomposite has good discrimination and would be suitable to analyze real samples without being greatly affected by matrix.

The selectivity of developed rGO/Fe_3O_4/TiO_2/GCE sensor was also assessed using DPV in presence of possible interfering species. Fig. 6 represents the DPV responses of 50 μM CAP in absence and presence of common interfering compounds like glucose, ascorbic acid, Mg^{2+}, and K^+ at concentrations up to 2-fold excess. The resulting electrochemical responses showed insignificant variations in cathodic peak current and peak potential of CAP.[57]

Quantitatively, changes in peak current were determined to be less than ±5%, and changes in peak potential were within ±10 mV, which showed little interference with coexisting species. These findings affirm that the sensor is highly selective to CAP even in complicated matrices. Such low interference could be explained by preferential adsorption of CAP on rGO surface through the π–π interaction and selectivity of Fe_3O_4 to reduce nitro group, which is absent in interfering molecules. The ternary heterostructure also enables selective electron transfer kinetics, which further increases level of discrimination against non-target species.

3.4.3 Reproducibility and stability. To test reproducibility of fabrication, a series of self-assembled rGO/Fe_3O_4/TiO_2 modified electrodes were subjected to same conditions. The low RSD of various electrodes proves consistency and dependability of synthesis and modification process. The consistent distribution of Fe_3O_4 and TiO_2 NPs across rGO sheets is associated with homogenous distribution of active sites and reproducible electrochemical characteristics. The reproducibility of developed sensor was checked by employing DPV, and it was found that the measurements of a 0.5 mM CAP solution with 5 independently fabricated electrodes had an RSD value of 1.79% (Fig. 7(a)). Meanwhile, the stability of developed sensor was also found by taking measurements of a 0.5 mM CAP solution with a fabricated electrode at once, after 1 hour, after a day, after a week, and after four weeks, with an RSD value of 3% as shown in Fig. 7(b). The permanence of modified electrode was tested with long-term storage stability of modified electrode in either ambient or refrigerated conditions.[58,59] The sensor still had a high percentage of its original current response following weeks/days of storage, showing good structural integrity and chemical stability of nanocomposite. The stability was increased because of strong bonding between metal oxides and rGO sheets. rGO prevents NPs from agglomerating, increases electron mobility, and decreases recombination of charges at heterointerface.[60] Moreover, we have repeated scans of cyclic voltammetry, resulting in very low current degradation, which proved that the sensing platform was

© 2026 The Author(s). Published by the Royal Society of Chemistry

Open Access Article. Published on 05 June 2026. Downloaded on 6/15/2026 10:28:08 PM.
This article is licensed under a Creative Commons Attribution 3.0 Unported Licence.

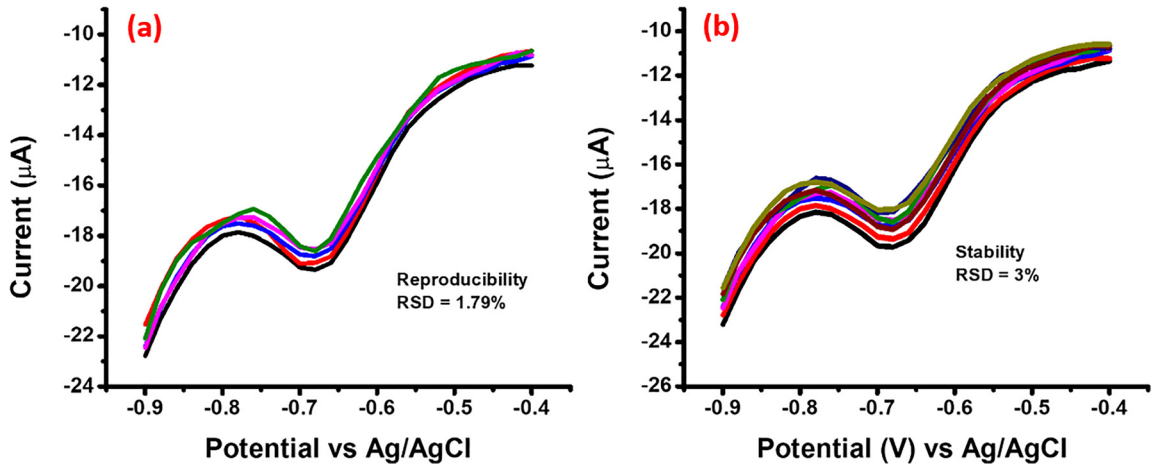

Fig. 7 (a) Reproducibility of rGO–Fe_3O_4/TiO_2/GCE, and (b) stability of rGO–Fe_3O_4/TiO_2/GCE.

Table 3 Designed sensor comparison of CAP with reported sensors

Electrode	Detection method	Redox response	Linear range (μM)	LOD (μM)	Ref.
AuNPs/GO	Amperometry	Oxidation	1.5–2.95	0.25	13
MoS_2/f-MWCNTs	Amperometry	Reduction	0.08–1392	0.02	61
Fe_3O_4–CMC@Au	SWV	Reduction	2.5–25	0.07	46
3DRGO/GCE	DPV	Reduction	1–113	0.15	49
Fe_3O_4/GCE	CV/SWV	Reduction	0.09–47	0.09	48
rGO–Fe_3O_4–TiO_2	CV/DPV	Reduction	2–100	0.88	Present work

electrochemically stable. In general, the high repeatability, reproducibility, and stability prove that rGO/Fe_3O_4/TiO_2 nanocomposite is a solid and stable electrocatalytic material that can find its way into practice in sensing.

3.5 Comparison of the designed sensor for CAP with reported sensors

The comparison of the rGO–Fe_3O_4/TiO_2 modified GCE has been done with the reported sensor, which indicates that our designed sensor produces comparable results with the already reported sensor, which is described in Table 3.

3.6 Proposed possible redox mechanism of CAP

The mechanism of electrochemical behavior of CAP can be explained as follows. The main reduction peak A can be attributed to four electron irreversible reduction of nitro group of chloramphenicol to the hydroxylamine group. Furthermore, two peaks B_1 and B_2 have been observed, which correspond to two electron reversible redox reaction of hydroxyl group to nitroso derivative of CAP as shown in Fig. 8(a and b). The electrochemical response of CAP at rGO–Fe_3O_4/TiO_2 modified electrode is primarily governed by reduction of its electroactive nitro (–NO_2) functional group. During cathodic scan, CAP undergoes a proton-coupled multi-electron transfer process in which nitro group is reduced to corresponding hydroxylamine (–NHOH) intermediate through a four-electron and four-proton pathway. This reduction step is responsible for well-defined cathodic peak observed in voltammetric profile. In subsequent anodic scanning, a reversible redox couple may appear due to interconversion between hydroxylamine (–NHOH) and nitroso (–NO) derivatives, indicating a quasi-reversible two-electron process. The enhanced electrocatalytic performance of rGO–Fe_3O_4/TiO_2 nanocomposite is attributed to synergistic interfacial effects: the π-conjugated network of rGO facilitates rapid electron transport and strong π–π interactions with aromatic ring of CAP; Fe_3O_4 NPs act as catalytic active centers that accelerate the reduction kinetics of nitro group; and TiO_2 contributes to improved adsorption and stabilization of reaction intermediates through surface hydroxyl groups.[62] The heterojunction interface between rGO, Fe_3O_4, and TiO_2 further lowers the charge-transfer resistance, enhances electron mobility, and promotes efficient proton-assisted reduction. Overall, sensing mechanism is dominated by adsorption-controlled electrocatalytic reduction of nitro group of CAP, facilitated by accelerated interfacial electron transfer within the ternary nanocomposite system.

The synergistic interfacial effects that enable transfer of charges and adsorption of analytes can explain improved sensing capabilities of ternary rGO–Fe_3O_4/TiO_2 nanocomposite. The rGO π-conjugated network, being highly conductive, affords efficient electron transport routes and fosters intense π-capacitance with aromatic framework of CAP, resulting in enhanced surface concentration of analyte. Fe_3O_4 NPs present themselves as redox-active catalytic centers, which reduce activation energy of reduction of nitro group, thus accelerating electron transfer kinetics. At the same time, TiO_2 also exhibits semiconducting properties and hydroxyl groups on surface that improve adsorption of CAP and stabilize the reaction

Open Access Article. Published on 05 June 2026. Downloaded on 6/15/2026 10:28:08 PM.
This article is licensed under a Creative Commons Attribution 3.0 Unported Licence.

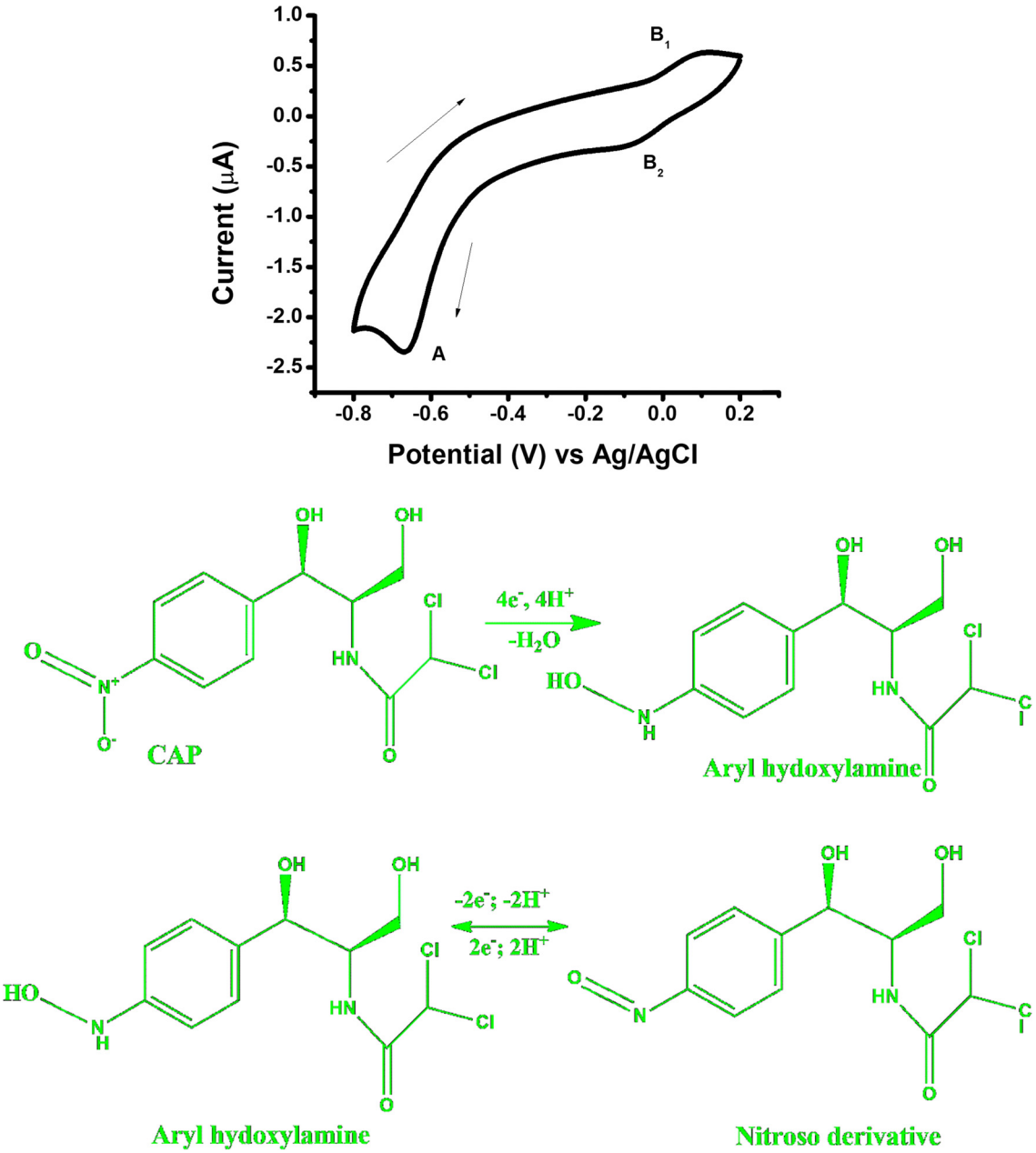

Fig. 8 (a) CV of rGO–Fe_3O_4/TiO_2/GCE in the presence of 0.2 mM CAP/PB at a scan rate of 100 mV, and (b) mechanism of the electrochemical behavior of CAP.

intermediates by hydrogen bonding and surface complexation. The close interfacial interaction between rGO, Fe_3O_4, and TiO_2 creates a heterostructured network that minimizes charge-transfer resistance, as demonstrated in EIS, and maximizes electroactive surface area, leading to enhanced current response. Besides, linearity of relationship between peak current and square of scan rate, which indicates diffusion control of process, implies that CAP molecules are carried to electrode surface efficiently in bulk solution, and electron transfer to electrode surface proceeds rapidly. In such a way, general sensing process will be a mixture of adsorption-enhanced accumulation, proton-coupled electron transfer, and catalytic reduction at active sites, which are promoted by synergistic action of ternary nanocomposite components.

4. Conclusion

A ternary rGO–Fe_3O_4/TiO_2 nanocomposite has been successfully prepared as a high-performance electrocatalyst to detect chloramphenicol. The conductive rGO was synthesized with Fe_3O_4 and TiO_2 NPs to produce a synergistic heterojunction structure, which allowed a fast transport of electrons and increased electrocatalytic reduction of CAP. The modified

© 2026 The Author(s). Published by the Royal Society of Chemistry

Open Access Article. Published on 05 June 2026. Downloaded on 6/15/2026 10:28:08 PM. This article is licensed under a Creative Commons Attribution 3.0 Unported Licence.

electrode was found to be more sensitive, and had a lower detection limit, better reproducibility, and a higher level of anti-interference than bare and binary-modified electrodes. The enhanced analytical performance is largely credited to enhanced electroactive surface area, enhanced charge-transfer kinetics, and high adsorption affinity of CAP on nanocomposite surface. These data prove that rGO–Fe_3O_4/TiO_2 needs a solid foundation to be developed as an effective and inexpensive electrochemical sensor to detect antibiotic residues.

• Further elucidation of charge-transfer mechanism and adsorption behavior of chloramphenicol on ternary interface should be done by advanced spectroscopic and electrochemical methods, *e.g.*, *in situ* EIS or XPS studies.

• On-site monitoring could be made possible by integrating developed sensing platform into portable or screen-printed systems using electrodes.

• Selectivity in presence of complex biological samples could be enhanced by incorporation of molecularly imprinted polymers or aptamer-based recognition elements to chloramphenicol.

• Future studies can investigate the possibility of detecting several antibiotics at once using same nanocomposite.

• Long-period stability testing under diverse storage and operating conditions is suggested to be carried out to confirm business viability.

Conflicts of interest

There are no conflicts to declare.

Data availability

Data will be provided upon reasonable request to authors.

References

1 S. Gao, *et al.*, Electrochemical chloramphenicol sensors-based on trace MoS_2 modified carbon nanomaterials: Insight into carbon supports, *J. Alloys Compd.*, 2021, **872**, 159687.
2 S. N. Karim, *et al.*, Innovative technological approaches in the detection and mitigation of food toxicants, *Food Rev. Int.*, 2025, 1–45.
3 S. Pakapongpan, *et al.*, A facile one-pot synthesis of magnetic iron oxide nanoparticles embed N-doped graphene modified magnetic screen printed electrode for electrochemical sensing of chloramphenicol and diethylstilbestrol, *Talanta*, 2022, **241**, 123184.
4 A. Munawar, *et al.*, Investigating nanohybrid material based on 3D CNTs@ Cu nanoparticle composite and imprinted polymer for highly selective detection of chloramphenicol, *J. Hazard. Mater.*, 2018, **342**, 96–106.
5 N. A. Shad, *et al.*, Solution growth of 1D zinc tungstate ($ZnWO_4$) nanowires; design, morphology, and electrochemical sensor fabrication for selective detection of chloramphenicol, *J. Hazard. Mater.*, 2019, **367**, 205–214.
6 C. Chang, *et al.*, Highly efficient detection of chloramphenicol in water using Ag and TiO_2 nanoparticles modified laser-induced graphene electrode, *Microchem. J.*, 2022, **173**, 107037.
7 P. S. Adarakatti, Fundamentals of electrochemistry, in *Agricultural electrochemistry*, 2025, ACS Publications. pp. 17–46.
8 R. Ullah, *et al.*, Electrochemical sensing of H_2O_2 using cobalt oxide modified TiO_2 nanotubes, *Curr. Appl. Phys.*, 2022, **38**, 40–48.
9 X. Qin, *et al.*, A ''signal-on'' photoelectrochemical aptasensor based on graphene quantum dots-sensitized TiO_2 nanotube arrays for sensitive detection of chloramphenicol, *Talanta*, 2019, **197**, 28–35.
10 Y. B. Chan, *et al.*, Review in green synthesis mechanisms, application, and future prospects for Garcinia mangostana L.(mangosteen)-derived nanoparticles, *Nanotechnol. Rev.*, 2025, **14**(1), 20250157.
11 S. I. Mohammad, *et al.*, Perovskite quantum dot-based gas sensors for environmental monitoring: mechanisms, materials, and perspectives on next-generation pollution control, *RSC Adv.*, 2025, **15**(55), 47476–47505.
12 J. He, *et al.*, Fabrication of MoS_2 loaded on expanded graphite matrix for high-efficiency pH-universal hydrogen evolution reaction, *J. Alloys Compd.*, 2020, **828**, 154370.
13 R. Karthik, *et al.*, Green synthesized gold nanoparticles decorated graphene oxide for sensitive determination of chloramphenicol in milk, powdered milk, honey and eye drops, *J. Colloid Interface Sci.*, 2016, **475**, 46–56.
14 R. B. Manami, *et al.*, Advancement in highly selective electrochemical sensing of Pb (II) using $CuWO_4$/RGO nanocomposite modified electrode, *J. Mater. Sci.: Mater. Electron.*, 2025, **36**(36), 2268.
15 K. Kor and K. Zarei, Electrochemical determination of chloramphenicol on glassy carbon electrode modified with multi-walled carbon nanotube–cetyltrimethylammonium bromide–poly (diphenylamine), *J. Electroanal. Chem.*, 2014, **733**, 39–46.
16 K. Abhishek, *et al.*, A review on nanomaterial based electrode for electrochemical detection of chloramphenicol and furazolidone antibiotics, *Anal. Methods*, 2022, 3228–3249.
17 J. R. Maluta, *et al.*, Development of a semigraphitic sulfur-doped ordered mesoporous carbon material for electroanalytical applications, *Sens. Actuators, B*, 2018, **257**, 347–353.
18 L. Xiao, *et al.*, Highly sensitive electrochemical sensor for chloramphenicol based on MOF derived exfoliated porous carbon, *Talanta*, 2017, **167**, 39–43.
19 P. S. Adarakatti and C. E. Banks, *Advances in electrochemical sensing and catalysis: bridging fundamentals and applications*, 2025.
20 N. Mariotti, *et al.*, Recent advances in eco-friendly and cost-effective materials towards sustainable dye-sensitized solar cells, *Green Chem.*, 2020, **22**(21), 7168–7218.
21 A. Scalia, *et al.*, A flexible and portable powerpack by solid-state supercapacitor and dye-sensitized solar cell integration, *J. Power Sources*, 2017, **359**, 311–321.

Open Access Article. Published on 05 June 2026. Downloaded on 6/15/2026 10:28:08 PM. This article is licensed under a Creative Commons Attribution 3.0 Unported Licence.

22 L. Cindrella, *et al.*, Gas diffusion layer for proton exchange membrane fuel cells—A review, *J. Power Sources*, 2009, **194**(1), 146–160.
23 W. Zhou, *et al.*, Anodes for Carbon-Fueled Solid Oxide Fuel Cells, *ChemElectroChem*, 2016, **3**(2), 193–203.
24 Z.-J. He, *et al.*, An electrochemiluminescence aptamer sensor for chloramphenicol based on GO-QDs nanocomposites and enzyme-linked aptamers, *J. Electroanal. Chem.*, 2020, **860**, 113870.
25 R. Yogeeshwari, *et al.*, Synthesis of acid resistant $Fe_2V_4O_{13}$-polypyrrole nanocomposite: its application towards the fabrication of disposable electrochemical sensor for the detection of As (III), *Mater. Res. Express*, 2019, **6**(12), 126448.
26 L. Geng, *et al.*, Molecularly imprinted electrochemical sensor based on multi-walled carbon nanotubes for specific recognition and determination of chloramphenicol in milk, *Microchem. J.*, 2022, **182**, 107887.
27 K. P. Mulaudji, *et al.*, Advancement in electrochemical sensing of chloramphenicol in varying matrixes: A review, *Talanta Open*, 2025, 100561.
28 A. Karthika, *et al.*, Electrochemical sensing of nicotine using $CuWO_4$ decorated reduced graphene oxide immobilized glassy carbon electrode, *Ultrason. Sonochem.*, 2019, **55**, 196–206.
29 K. Venkatesh, *et al.*, Spinel $CoMn_2O_4$ nano-/micro-spheres embedded RGO nanosheets modified disposable electrode for the highly sensitive electrochemical detection of metol, *J. Ind. Eng. Chem.*, 2022, **106**, 287–296.
30 P. Karuppasamy, *et al.*, An investigation of transition metal doped TiO_2 photocatalysts for the enhanced photocatalytic decoloration of methylene blue dye under visible light irradiation, *J. Environ. Chem. Eng.*, 2021, **9**(4), 105254.
31 P. Karuppasamy, *et al.*, An efficient and highly sensitive amperometric quercetin sensor based on a lotus flower like SeO_2-decorated rGO nanocomposite modified glassy carbon electrode, *Electrocatalysis*, 2022, **13**(3), 269–282.
32 F. Dehdashti, *et al.*, Facile and green synthesis of α-Fe_2O_3 nanoparticles stabilized with chitosan for phototherapy with 808 nm laser irradiation, *Sci. Rep.*, 2025, **15**(1), 32269.
33 S. U. Rehman, Y.-H. Lin and H.-F. Wu, Oxygen-Deficient Fluorescent λ-MnO_2 Nanosheets for Selective Detection of Chloramphenicol, *ACS Appl. Nano Mater.*, 2025, **8**(20), 10306–10314.
34 I. Kumar, *et al.*, Fabrication of α-Fe_2O_3 nanostructures: synthesis, characterization, and their promising application in the treatment of carcinoma A549 lung cancer cells, *ACS Omega*, 2022, **7**(25), 21882–21890.
35 J. Chen, *et al.*, An improved Hummers' method for eco-friendly synthesis of graphene oxide, *Carbon*, 2013, **64**, 225–229.
36 E. Andrijanto, *et al.*, Facile synthesis of graphene from graphite using ascorbic acid as reducing agent, in *AIP Conference Proceedings*, 2016, AIP Publishing LLC.
37 S. Bibi, *et al.*, Photocatalytic degradation of malachite green and methylene blue over reduced graphene oxide (rGO) based metal oxides (rGO-Fe_3O_4/TiO_2) nanocomposite under UV-visible light irradiation, *J. Environ. Chem. Eng.*, 2021, **9**(4), 105580.
38 A. Karthika, *et al.*, Green synthesized CaO decorated ternary CaO/g-C_3N_4/PVA nanocomposite modified glassy carbon electrode for enhanced electrochemical detection of caffeic acid, *Sci. Rep.*, 2024, **14**(1), 28714.
39 R. Nehru, *et al.*, Nanoscale Mn_3O_4 electrocatalyst as improved electrode materials for electrochemical sensing of chloramphenicol drug. ACS Applied Nano, *Materials*, 2023, **6**(2), 1235–1249.
40 S. Salagare, *et al.*, A selective electrochemical sensor based on titanium dioxide-reduced graphene oxide nanocomposite (TiO_2-RGO/GCE) for the efficient determination of nitrite, *Mater. Res. Innovations*, 2023, **27**(1), 33–44.
41 N. X. Dinh, *et al.*, Ultrasensitive determination of chloramphenicol in pork and chicken meat samples using a portable electrochemical sensor: effects of 2D nanomaterials on the sensing performance and stability, *New J. Chem.*, 2021, **45**(17), 7622–7636.
42 J. Mehralipour, S. Bagheri and M. Gholami, Synthesis and characterization of rGO/Fe_0/Fe_3O_4/TiO_2 nanocomposite and application of photocatalytic process in the decomposition of penicillin G from aqueous, *Heliyon*, 2023, **9**(7), e18172.
43 R. D. Crapnell, P. S. Adarakatti and C. E. Banks, Electroanalytical overview: the electroanalytical detection of oxalate, *Sens. Actuators, Rep.*, 2023, **6**, 100176.
44 S. Bunnasit, *et al.*, Sensitive portable electrochemical sensors for antibiotic chloramphenicol by tin/reduced graphene oxide-modified screen-printed carbon electrodes, *ACS Appl. Nano Mater.*, 2024, **7**(1), 267–278.
45 C. Chen, *et al.*, Highly sensitive and selective electrochemical sensor for the determination of chloramphenicol, *J. Food Compos. Anal.*, 2024, **129**, 106114.
46 P. Jakubec, *et al.*, Advanced sensing of antibiotics with magnetic gold nanocomposite: electrochemical detection of chloramphenicol, *Chem. – Eur. J.*, 2016, **22**(40), 14279–14284.
47 P. S. Adarakatti, R. D. Crapnell and C. E. Banks, Electroanalytical overview: the sensing of hydroxylamine, *Anal. Methods*, 2023, **15**(22), 2709–2720.
48 K. Giribabu, *et al.*, Electrochemical determination of chloramphenicol using a glassy carbon electrode modified with dendrite-like Fe_3O_4 nanoparticles, *Carbon Lett.*, 2017, **23**, 38–47.
49 X. Zhang, Y.-C. Zhang and J.-W. Zhang, A highly selective electrochemical sensor for chloramphenicol based on three-dimensional reduced graphene oxide architectures, *Talanta*, 2016, **161**, 567–573.
50 R. Karthik, *et al.*, A study of electrocatalytic and photocatalytic activity of cerium molybdate nanocubes decorated graphene oxide for the sensing and degradation of antibiotic drug chloramphenicol, *ACS Appl. Mater. Interfaces*, 2017, **9**(7), 6547–6559.
51 Y. Yuan, *et al.*, A sensor based on Au nanoparticles/carbon nitride/graphene composites for the detection of chloramphenicol and ciprofloxacin, *ECS J. Solid State Sci. Technol.*, 2018, **7**(12), M201–M208.

© 2026 The Author(s). Published by the Royal Society of Chemistry

Open Access Article. Published on 05 June 2026. Downloaded on 6/15/2026 10:28:08 PM.
This article is licensed under a Creative Commons Attribution 3.0 Unported Licence.

52 Y. Sun, J. Zhao and L. Liang, Recent development of antibiotic detection in food and environment: the combination of sensors and nanomaterials, *Microchim. Acta*, 2021, **188**(1), 21.

53 A. Lochab, *et al.*, Conductive polymer based MWCNTs nanocomposite as electrochemical sensing platform to detect chloramphenicol, *Synth. Met.*, 2023, **297**, 117397.

54 V. Vinothkumar, M. Abinaya and S.-M. Chen, Ultrasonic assisted preparation of $CoMoO_4$ nanoparticles modified electrochemical sensor for chloramphenicol determination, *J. Solid State Chem.*, 2021, **302**, 122392.

55 R. Singhaal, S. Devi and H. N. Sheikh, Synergistic nanomaterial system for luminescence sensing of MnO_4-anion and enhanced photocatalytic removal of antibiotic chloramphenicol (CAP) in aqueous environments using Dy^{3+}/Tb^{3+} co-doped $NaYF_4$ and graphene oxide hybrid, *J. Alloys Compd.*, 2024, **1002**, 175332.

56 N. H. Anh, *et al.*, Gold nanoparticles-based SERS nanosensor for thiram and chloramphenicol monitoring in food samples: Insight into effects of analyte molecular structure on their sensing performance and signal enhancement, *Appl. Surf. Sci.*, 2022, **584**, 152555.

57 H. Guo, *et al.*, Accelerated Fenton reaction for antibiotic ofloxacin degradation in discharge plasma system based on graphene-Fe_3O_4 nanocomposites, *Vacuum*, 2021, **185**, 110022.

58 Y. Liu, *et al.*, Defective Se-doped In_2S_3 nanomaterial-based photoelectrochemical biosensor for the ultrasensitive detection of chloramphenicol, *Sens. Actuators, B*, 2022, **373**, 132705.

59 N. T. Vinh, *et al.*, Dual-functional sensing properties of $ZnFe_2O_4$ nanoparticles for detection of the chloramphenicol antibiotic and sulphur dioxide gas, *Sens. Actuators, A*, 2021, **332**, 113093.

60 L. Zhang, *et al.*, Synthesis of rGO@ PDA@ AuNPs for an effective electrochemical chloramphenicol sensor, *Diamond Relat. Mater.*, 2022, **128**, 109311.

61 M. Govindasamy, *et al.*, Molybdenum disulfide nanosheets coated multiwalled carbon nanotubes composite for highly sensitive determination of chloramphenicol in food samples milk, honey and powdered milk, *J. Colloid Interface Sci.*, 2017, **485**, 129–136.

62 Q. Gu, *et al.*, Nitrogen-doped graphdiyne quantum dots for electrochemical chloramphenicol quantification in water, *ACS Appl. Nano Mater.*, 2021, **4**(11), 12755–12765.